JACS
JOURNAL OF THE AMERICAN CHEMICAL SOCIETY
Article
pubs.acs.org/JACS

Substrate-Assisted Catalytic Mechanism of *O*-GlcNAc Transferase Discovered by Quantum Mechanics/Molecular Mechanics Investigation

Igor Tvaroška,*[,†,‡] Stanislav Kozmon,[‡,§,⊥] Michaela Wimmerová,[‡,§] and Jaroslav Koča[‡,§]

[†]Institute of Chemistry, Slovak Academy of Sciences, 845 38 Bratislava, Slovak Republic
[‡]Central European Institute of Technology (CEITEC), Masaryk University, 625 00 Brno, Czech Republic
[§]National Centre for Biomolecular Research, Faculty of Science, Masaryk University, 625 00 Brno, Czech Republic

Supporting Information

ABSTRACT: In higher eukaryotes, a variety of proteins are post-translationally modified by adding *O*-linked *N*-acetylglucosamine (GlcNAc) residue to serine or threonine residues. Misregulation of *O*-GlcNAcylation is linked to a wide variety of diseases, such as diabetes, cancer, and neurodegenerative diseases, including Alzheimer's disease. GlcNAc transfer is catalyzed by an inverting glycosyltransferase *O*-GlcNAc transferase (uridine diphospho-*N*-acetylglucosamine:polypeptide *β*-*N*-acetylaminyltransferase, OGT) that belongs to the GT-B superfamily. The catalytic mechanism of this metal-independent glycosyltransferase is of primary importance and is investigated here using QM(DFT)/MM methods. The structural model of the reaction site used in this paper is based on the crystal structures of OGT. The entire enzyme−substrate system was partitioned into two different subsystems: the QM subsystem containing 198 atoms, and the MM region containing 11 326 atoms. The catalytic mechanism was monitored by means of three two-dimensional potential energy maps calculated as a function of three predefined reaction coordinates at different levels of theory. These potential energy surfaces revealed the existence of a concerted S_N2-like mechanism, in which a nucleophilic attack by O_{Ser}, facilitated by proton transfer to the catalytic base, and the dissociation of the leaving group occur almost simultaneously. The transition state for the proposed reaction mechanism at the MPW1K level was located at C1−O_{Ser} = 1.92 Å and C1−O1 = 3.11 Å. The activation energy for this passage was estimated to be ∼20 kcal mol^{-1}. These calculations also identified, for the first time for glycosyltransferases, the substrate-assisted mechanism in which the *N*-acetamino group of the donor participates in the catalytic mechanism.

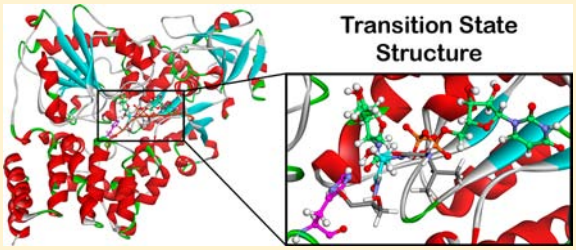

INTRODUCTION

The post-translational modification of serines or threonines on proteins by *O*-linked *N*-acetylglucosamine (GlcNAc)[1] regulates a wide range of cellular processes[2−4] and plays a key role in regulating gene expression, both at the transcriptional and translational levels.[5] *O*-GlcNAcylation is truly dynamic[6] and is balanced by just two distinct enzymes that are responsible for the *O*-GlcNAc cycling in human,[7,8] namely inverting glycosyltransferase *O*-GlcNAc transferase (uridine diphospho-*N*-acetylglucosamine:polypeptide *β*-*N*-acetylaminyltransferase, OGT) and glycoside hydrolase *O*-GlcNAcase (OGA), also known as hexaminidase C (HexC).[9] Glycosyltransferase OGT catalyzes the addition of *O*-linked *N*-acetylglucosamine from UDP-GlcNAc (uridine diphospho-*N*-acetylglucosamine) onto the hydroxyl group of a serine or a threonine residue on protein substrates (Scheme 1). OGT is a metal-independent enzyme and operates via an inverting mechanism. In contrast, the glycoside hydrolase OGA is responsible for the removal of the *O*-*β*-linked GlcNAc from the serine or threonine moiety of modified proteins. *O*-*β*-Glycosidic transfer by OGT differs from classical glycosylation in that the GlcNAc monosaccharide residue is not further modified or elongated into complex oligosaccharide structures.[1] Since many *O*-GlcNAcylation sites are also phosphorylation sites, OGT plays a pivotal role in

Scheme 1. Schematic Diagram of the Enzymatic Reaction Catalyzed by OGT

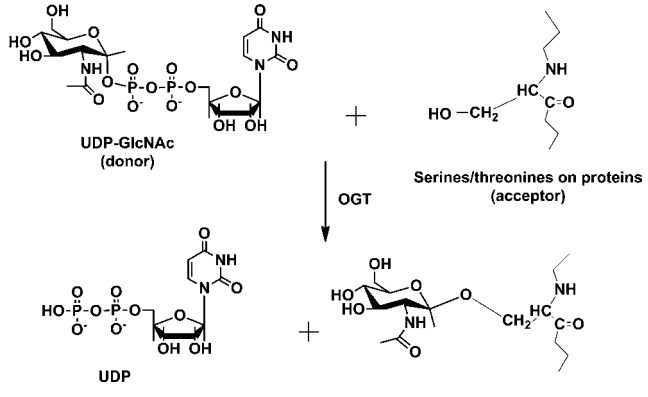

Received: July 18, 2012
Published: August 28, 2012

modulating cellular kinase signaling cascades.[10,11] There is a considerable amount of evidence[4] suggesting that aberrant OGT *O*-GlcNAcylation is associated with diabetes, cancer, and neurodegenerative diseases, including Alzheimer's disease. In terms of primary sequences, OGT belongs to the GT41 family in the CAZY database.[12] Based on the sequence analysis, OGT was predicted to be a member of the GT-B superfamily of glycosyltransferases.[13]

Recently, two structures of a human OGT containing 4.5 tetratricopeptide repeat (TPR) units and the catalytic domain (hOGT4.5) were determined.[14] The catalytic properties of this construct were found to be similar to those of the full-length enzyme. One structure was the complex with UDP (PDB code 3PE3) resolved at 2.8 Å; the second structure was a complex containing UDP and a well-characterized acceptor, 14-residue CKII peptide substrate (YPGGSTPVS*SANMM; glycosylated serine is referred to as S*, PDB code 3PE4), resolved at 1.95 Å. In these structures, the catalytic region contains three domains: the amino N-terminal domain, the carboxy C-terminal domain, and the intervening domain. The N-terminal and C-terminal domains have the Rossmann-like fold typical of GT-B superfamily members. However, the N-terminal domain is unique in containing two additional helices, H1 and H2, which form an essential part of the active site. In the OGT-UDP-peptide complex, the UDP moiety binds in a pocket in the C-terminal domain near the interface with the N-terminal domain. Histidine 498, which is located between the reactive serine hydroxyl and GlcNAc, was found to be critical for the activity of OGT and was proposed to be the catalytic base. OGT-UDP crystallized with four copies in the asymmetric unit, and OGT-UDP-CKII crystallized as a dimer. However, these multimerizations do not seem to be physiologically relevant, since it has been shown that the construct is monomeric in solution.[14]

Though the recently resolved crystal structures of OGT significantly increased our understanding of the mechanism of *O*-GlcNAcylation, many fundamental questions have still not been addressed, and the exact catalytic mechanism of OGT remains to be understood. Experimental data[15] and theoretical calculations[16−19] on inverting glycosyltransferases with the GT-A fold support a concerted S_N2-like mechanism facilitated by a general base. The role of the metal is to assist in the departure of the leaving group. To our knowledge, a theoretical investigation of the mechanism of GT with the GT-B fold has not been conducted. The availability of the OGT crystal structure prompted us to examine the catalytic mechanism of OGT at the microscopic level. Since OGT is a metal-independent enzyme, and the acceptor is not a carbohydrate but an amino acid, the question remains of which form OGT uses to promote the breaking of the glycosidic linkage and the departure of nucleoside diphosphate leaving group. An important outcome of this study is the establishment of the transition-state structure. This could serve as a guide in designing powerful and specific inhibitors.

MODELS AND METHODS

Model Preparation. The coordinates of the OGT-UDP-peptide complex were obtained from the PDB database under the code 3PE4, and prepared using Modeller,[20,21] UCSF Chimera,[22] Schrodinger's Maestro,[23] and Protein Preparation Wizard[24−27] from the Schrodinger suite of programs as follows. All molecules labeled "A" in the PDB data were selected. All water oxygen atoms were removed from the structure before the missing residues were added. The missing amino acids residues Ser715−His718 (4 residues) and Lys747−Ala761 (14 residues) were added by Modeller so that all atoms from the original PDB data were fixed to their original coordinates and only the added amino acid residue in the loops were optimized. Afterward, hydrogen atoms were added, and protonation states were assigned on the basis of the residue pK_a value at normal pH (7.0). The orientations of the added hydrogen atoms and protonation of the histidine residues were based on the positions and types of the neighboring atoms using the method implemented in UCSF Chimera. The His498 residue was protonized in the neutral form correctly to the δ-position of the histidine ring. The protonized structure was used for docking the missing active donor substrate UDP-GlcNAc. A docking grid was prepared using Maestro GUI[23] and Glide.[28−32] Atom types and partial charges were assigned according to the OPLS_2005 force field, also known as OPLS-AA.[33] The structure of UDP-GlcNAc was obtained by energy minimization using Jaguar program v9.034 at the density functional theory (DFT) B3LYP[35,36] level with the 6-31+G* basis set prior to docking. The calculated electrostatic potential fit (ESP) charges were used as input partial charges for ligand atoms in the docking calculations. A docking grid was generated for the prepared OGT-UDP-peptide structure, with the center of the cubic grid box placed on the centroid of the bound UDP. The box size was set to 12 Å in all three dimensions. Three constraints were defined for the docking. The first constraint was set to the geometrical center of the uracil ring, and the remaining two constraints were set to the position of the phosphor atoms in the diphosphate moiety. The UDP-GlcNAc molecule was then docked into the active site using Glide with standard parameters for the standard precision docking and defined contraints set. A docked pose was chosen for UDP-GlcNAc with the proper orientation of the UDP moiety and a reasonable distance of the GlcNAc anomeric carbon from the acceptor, Ser21 from the CKII peptide sequence. The OGT-UDP-GlcNAc-peptide ternary complex was overlaid with the original crystal structure with water oxygen atoms. All oxygen atoms with low *B*-factors were visualized in a 10 Å area around the UDP-GlcNAc. The 23 water oxygen atoms with possible non-covalent interactions with ligands (water residues 4, 12, 14, 20, 29, 48, 54, 56, 59, 73, 147, 201, 217, 219, 284, 325, 384, 409, 413, 414, 415, 417, and 422) were retained in the active site. Water oxygen atoms were protonized, and then water molecules were oriented to generate the appropriate interactions with neighboring atoms.

QM/MM Model. The QM/MM calculations were carried out using the program Schrodinger's QSite.[37−39] In the Qsite, the QM/MM methodology (an additive scheme) was employed with frozen atoms and with electrostatic treatment at the interface between QM and MM regions using Gaussian charge distribution represented on a grid. The entire enzyme−substrate system (OGT-UDP-GlcNAc-CKII peptide ternary complex), consisting of 713 amino acids, 23 water molecules, donor, and acceptor (altogether 11 524 atoms), was partitioned into two different subsystems: the QM and the MM regions. The QM subsystem, containing 198 atoms, was formed of a complete donor, UDP-GlcNAc; three complete residues of the acceptor CKII peptide, namely, Val20, Ser21 (nucleophile residue), and Ser22; and the side chains of the amino acids crucial for catalytic activity, His498 (suggested catalytic base), His558, Gln839, Lys842, Lys898, His901, and His920. Also, three water molecules (W4, W48, and W201) in the vicinity of UDP-GlcNAc were added into the QM region. The MM region (11 326 atoms) was composed of the remaining OGT and CK-II peptide atoms, and 20 water molecules presented in the model complex. Prior to the potential energy surface (PES) calculations, a geometry optimization of the whole structure was performed in order to obtain a refined location of the donor. The structure of the OGT-UDP-GlcNAc-CKII-peptide complex generated by the above procedure was optimized using dynamic constraints of 3.0 and 2.0 Å on the $O_{Ser21}\cdots C1$ and $H_{Ser21}\cdots N_{His498}$ distances, respectively. In this optimization, the QM subsystem was treated using DFT with the B3LYP[35,36] functional and 6-31G** basis set with diffuse functions (6-31+G**) on O1′, O5′, O_{Ser21}, and N_{His498} atoms from the Jaguar library,[34] and the MM subsystem was characterized with an OPLS_2005 all-atom force field.[33] The calculated structure was then used as the starting structure (Michaelis complex) for modeling the reaction catalyzed by OGT and is shown in Figure 1.

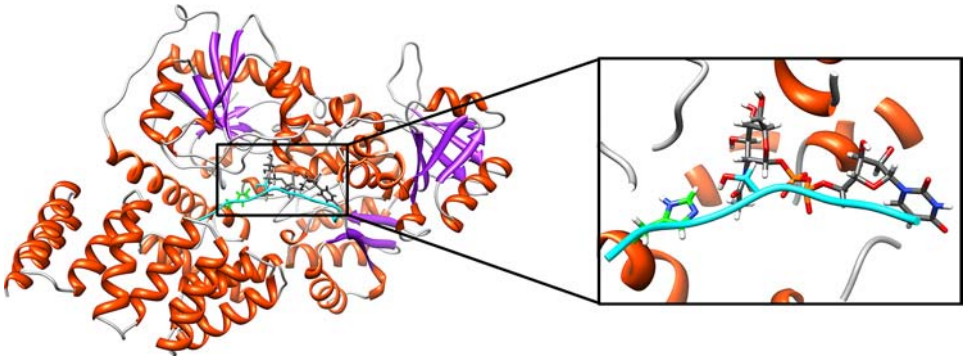

Figure 1. Ribbon representation of overall structure of human OGT-UDP-GlcNAc-CKII-peptide complex calculated using a QM/MM method with constraints of 3 and 2 Å on r_1 and r_2, respectively. Water molecules are not shown for clarity. Residues included in the QM region (UDP-GlcNAc, His498, and Ser21) for the QM/MM calculations are shown in stick representation.

Reaction Mechanism. The catalytic site chemistry of OGT involves the formation of a new glycosidic linkage between the serine acceptor (Ser21) and the anomeric carbon C1 of the donor GlcNAc, cleavage of the donor glycosidic linkage between GlcNAc and UDP, and a transfer of the H_{Ser} proton from the acceptor hydroxyl $O_{Ser}H_{Ser}$ to a catalytic base (His498). The reaction mechanism was monitored using three reaction coordinates. The first reaction coordinate r_1 was defined as the distance between the anomeric carbon C1 and the nucleophile oxygen O_{Ser} of the acceptor hydroxyl group. This reaction coordinate represented the nucleophilic attack of the serine acceptor on the anomeric carbon of the donor UDP-GlcNAc, and the result is the formation a new β-glycosidic linkage. The second reaction coordinate r_2 represented the dissociation of the glycosidic bond C1−O1 and was defined as the distance between the anomeric carbon C1 and glycosidic oxygen O1 of the donor UDP-GlcNAc. The third reaction coordinate r_3 represented the transfer of the proton from the nucleophile hydroxyl to the nitrogen of the catalytic base (His498) and was defined as the distance between the proton of the serine hydroxyl group H_{Ser} and the nitrogen of histidine N_{His}. All three coordinates are depicted in Figure 2, which only shows the QM region.

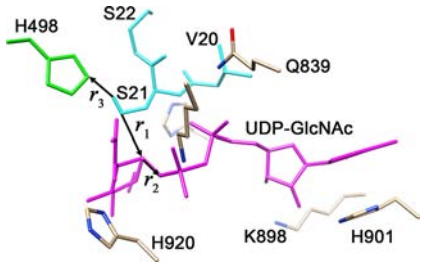

Figure 2. View of the QM region of the OGT-UDP-GlcNAc-CKII-peptide complex in stick representation. The QM region contains complete UDP-GlcNAc (in magenta); three whole residues of the CKII peptide (in cyan), namely Val20, Ser21 (acceptor), and Ser22; and side chains of amino acids crucial for the catalytic activity: H498 (suggested catalytic base, in green), His558, Gln839, Lys842, Lys898, His901, and His920 (in tan). There are also three water molecules in the vicinity of UDP-GlcNAc (not shown for clarity). The QM region consists of 198 atoms. The reaction coordinates r_1, r_2, and r_3 are depicted as arrows.

The reaction PES was determined by so-called adiabatic mapping. The reaction coordinates were varied by increments of 0.2 Å, between 3.5 and 1.4 Å for r_1 and r_2, and between 2.0 and 1.0 Å for r_3, respectively. In the vicinity of the barriers, the increment was decreased to 0.1 Å and then 0.05 Å. All the geometrical variables were optimized except for the reaction coordinates. The two-dimensional PES was calculated using DFT with the B3LYP[35,36] functional and 6-31G** basis set, with diffuse functions on O1′, O5′, O_{Ser21}, and N_{His498} from the Jaguar library[34] for the QM region and with the OPLS_2005 all-atom force field[33] for the MM region. In these calculations, to avoid extraordinarily extensive calculations, the optimizations were stopped after 150 geometry optimization steps, providing that the gradient rms was lower than 0.0005. Once the energy profile was obtained, the structure of the energetic maximum was used to search for the transition state using default criteria for this computation in QSite.[37−39] For the S_N2-like reaction path, the structures of Michaelis complex (ES), transition state (TS), and product complex (P) were optimized using B3LYP, M06-2X,[40] and MPW1K[41] functionals, and the basis set was as defined above. In addition, single-point calculations were carried out for these stationary points using various DFT functionals: the B3LYP, M06-2X, MPW1K, PWB6K,[42] and M05-2X.[43] The M06-2X, MPW1K, PWB6K, and M05-2X functionals should provide reasonable barrier heights and TS geometries for large systems.[44,45]

RESULTS AND DISCUSSION

The PES for the active-site chemical reaction was modeled using three reaction coordinates that represent the formation a new β-glycosidic linkage (r_1), cleavage of the C1−O1 glycosidic bond (r_2), and proton transfer (r_3) from the nucleophile to the catalytic base. Even in this arrangement, scanning the complete PES would have required an excessive amount of geometry optimizations (15×15×10) for such a complex system if all 2250 were not done. Therefore, to investigate the possible reaction pathways, we calculated three two-dimensional sections of the three-dimensional PESs, namely (r_1,r_2), (r_1,r_3), and (r_2,r_3). Even using this approach, the number of optimized structures exceeded 600. We note that a third reaction coordinate was also optimized during these calculations; e.g., for each point on the (r_1,r_3) map, the r_2 reaction coordinate (the C1−O1 distance) was allowed to relax, etc. The calculated PESs of the catalytic reactions are represented in the form of two-dimensional reaction coordinate contour diagrams in Figures 3−5. Different reaction pathways can be identified on these sections of the PES. The reaction pathways parallel to the vertical and horizontal axes denote individual steps in a stepwise mechanism, while the reaction pathways following the diagonal across the PES represent a concerted mechanism. Figure 6 shows the optimized structures of the active-site models in the ES, TS, and P complexes. The TS structure calculated with the MPW1K functional is given in Figure 7. Selected geometrical parameters and ESP charges for ES, TS, and P are listed in Table 1, and the relative energies of these stationary structures calculated at various levels of theory are given in Table 2.

dx.doi.org/10.1021/ja307040m | J. Am. Chem. Soc. 2012, 134, 15563−15571

PES as a Function of the r_1 ($r_{C1-O_{Ser}}$) and r_3 ($r_{H_{Ser}-N_{His}}$) Distances. Figure 3 shows the PES calculated in terms of the distance between the C1 and the O_{Ser} oxygen atom of the attacking serine residue (r_1) and the distance between the H_{Ser} proton and N_{His} nitrogen atom of the catalytic base (r_3). On this contour diagram, the horizontal axis represents the formation of the C−O glycosidic bond, while the vertical axis represents the proton transfer to histidine. The Michaelis complex is located in the upper right corner of the PES. Based on the model, it would be expected that the structures located in the upper and lower left corners are structures where the C2, O1, O5, O_{Ser}, and H1 atoms are bound to the anomeric carbon C1. These stationary points with penta-coordinated anomeric carbon should correspond to unstable high-energy structures. However, two low-energy regions were found in these locations. A thorough examination of the geometrical parameters of the points on the PES clearly revealed, as was observed in our previous studies,[18,46] that the C1−O1 length (r_2) varies in a continuous manner with the C1−O_{Ser} distance (r_1). As the nucleophilic attack on the anomeric carbon advances, the dissociation of the C1−O1 linkage simultaneously progresses. An examination of geometries showed that the most significant change in the C1−O1 distance occurred for a C1−O_{ser} distance between 2.4 and 2.0 Å. In this stage of the nucleophilic attack, the C1−O1 linkage elongates from 1.498 to 3.044 Å. Consequently, the structure located in the lower left corner corresponds to the product (P), while the structure in the upper left corner refers to the product with the protonated oxygen O_{Ser} and a formal +1 charge. The structure in the lower right corner corresponds to the ES with the H_{Ser} proton transferred from O_{Ser} to the catalytic base His498.

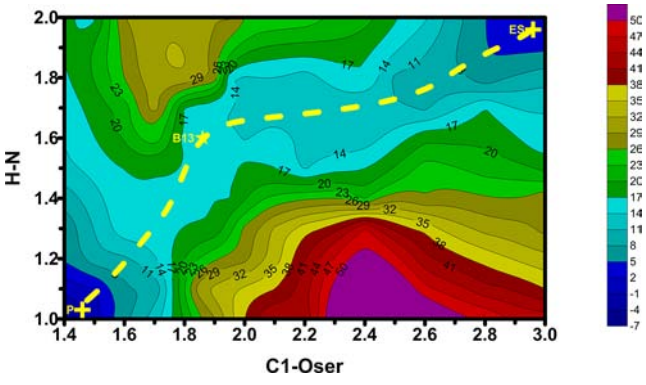

Figure 3. PES calculated at the B3LYP/6-31G* level using distances r_1 and r_3 as reaction coordinates. The yellow dashed line from the upper right corner to the bottom left corner indicates the S_N2-like reaction pathway from the ES to the P via the B13.

The PES given in Figure 3 shows the presence of one reaction pathway with a single transition barrier (B13) in the central region of the map and on the diagonal going from the Michaelis complex (ES) to the products (P). In this pathway, ES→B13→P, the presence of only one transition barrier indicates the existence of a concerted S_N2-like mechanism, in which the nucleophilic attack by O_{Ser} (r_1) facilitated by the proton transfer to the catalytic base (r_2) and the dissociation of the leaving group (r_3) all occur almost simultaneously. A key factor in the S_N2-like mechanism appears to be the nucleophilic attack, with the nucleophilicity of Ser21 hydroxyl increased by proton transfer to His498, functioning as the catalytic base.

Structural changes associated with the active-site chemical reaction are reflected in the structure of the points along the reaction pathways. As expected, an examination of the geometrical changes showed that the nucleophilic attack significantly alters the structure of UDP-GlcNAc. Optimized structures of the various stationary points found along the reaction pathways determined at the B3LYP level are shown below in Figure 6, and selected geometrical parameters are given in Table 1. The geometry of the ES model at the B3LYP level is characterized by values of 1.461 and 1.379 Å for the C1−O1 and C1−O5 bond lengths, respectively. The pyranoid ring of the GlcNAc is in the $^4C_1$ chair conformation, characterized by ring-puckering parameters ϕ = 140.1°, θ = 11.3°, and Q = 0.50, within normal $^4C_1$ values for θ but a bit flatter than normal for Q. B13 for this path occurs at the C1−O_{Ser} distance $r_1 \approx 1.8$ Å and $r_3 \approx 1.6$ Å. Along the concerted reaction path R (0.0 kcal mol^{-1}) → B13 (16 kcal mol^{-1}) → P (−1 kcal mol^{-1}), the conformation of the pyranoid ring continuously changes from a $^4C_1$ chair in ES through a $^4H_3$ half-chair in B13, with puckering parameters ϕ = 192.3°, θ = 69.4°, and Q = 0.57, back to a $^4C_1$ chair (100.4°, 3.7°, 0.59) conformation. In this process, the C1−O1 bond length between the anomeric carbon C1 and the leaving group, UDP, gradually elongates from 1.461 to 3.214 Å as the distance between the anomeric carbon and the attacking oxygen, r_1, decreases. The structure at the energy maximum (B13) was used to refine the structure of the TS without any geometry constraints. A TS search at the B3LYP level led to the TS structure characterized by the distances r_1 = 1.842 Å, r_2 = 3.214 Å, and r_3= 1.610 Å. Based on structural characteristics, the TS can be categorized as a late transition state.[47] (Atomic coordinates for the stationary points calculated at the B3LYP, MPW1K, and M06-2X levels are available in the Supporting Information.)

A comparison of the orientations of the *N*-acetyl (NAc) group revealed a particularly interesting behavior of the acetamido group. This group is in its most stable conformation, called the *Z-trans*.[48] However, along the reaction path, the *N*-acetyl group rotates around the C2−N linkage. In the ES, the conformation is characterized by the dihedral angle χ = 145° (χ = H2−C2−N−H_{NAc}), whereas the NAc group rotates to a conformation with χ = 175° in the TS. Although this is a relatively small conformational change, it brings the H_{NAc} proton near to the glycosidic oxygen O1, and the H_{NAc}−O1 distance decreases from 2.97 Å in the ES to 1.81 Å in the TS. As a result, the H_{NAc} proton interacts by hydrogen-bonding with the oxygen of the breaking glycosidic linkage. This interaction is supported by a charge development on the anomeric carbon O1 and the H_{NAc} proton during reaction (Table 1).

PES as a Function of the r_1 ($r_{C1-O_{Ser}}$) and r_2 (r_{C1-O1}) Distances. The PES calculated as a function of the distance (r_1) between the C1 and the O_{Ser} oxygen atom of the attacking serine residue, and the distance (r_2) between the anomeric carbon C1 and the glycosidic oxygen O1, is represented in Figure 4.

The structures in the lower left and the upper right corners represent the penta-coordinated anomeric carbon and the oxocarbenium ion, respectively. These structures appear to be high-energy structures with the penta-coordinated anomeric carbon corresponding, as expected, to the highest energy structure. Two distinct pathways can be seen on this contour

dx.doi.org/10.1021/ja307040m | J. Am. Chem. Soc. 2012, 134, 15563−15571

Table 1. QM/MM Calculated Geometrical Parameters (Distances in Å, Angles in Degrees) and Selected ESP Charges (Q, in e) of the Michaelis Complex (ES), Transition State (TS), and Product Complex (P) Observed on the Reaction Pathway Described in Figure 3 at B3LYP, MPW1K, and M06-2X Levels and 6-31G Basis Set with Diffuse Functions on O1′, O5′, O_{Ser21}, and N_{His498} (6-31+G**) Atoms**

	ES			TS			PC		
	B3LYP	MPW1K	M06-2X	B3LYP	MPW1K	M06-2X	B3LYP	MPW1K	M06-2X
r_1(C1−O_{Ser})	3.000	3.000	3.000	1.842	1.924	1.819	1.410	1.390	1.401
r_2(C1−O1)	1.461	1.436	1.444	3.214	3.109	3.173	3.409	3.347	3.363
r_3(N_{His}−H_{Ser})	2.000	2.000	2.000	1.610	1.679	1.613	1.033	1.024	1.030
O_{Ser}−N_{His}	2.891	2.894	2.883	2.663	2.691	2.664	3.676	3.690	3.531
C1−O5	1.379	1.367	1.377	1.307	1.278	1.303	1.411	1.390	1.400
H_{NAc}−O1	2.965	2.974	2.951	1.812	1.789	1.801	1.743	1.712	1.676
O5−C1−O_{Ser}	68.3	68.9	67.9	101.6	99.3	101.7	106.7	107.0	106.4
O5−C1−O1	110.9	111.1	111.2	85.4	88.2	85.4	138.5	138.7	137.4
O5−C1−H1	107.3	107.3	107.3	111.5	113.3	111.8	109.8	109.9	110.1
O5−C1−C2	111.3	110.9	110.8	119.7	120.8	119.1	110.5	110.6	111.2
O_{Ser}−C1−O1	144.0	142.4	143.9	156.6	154.9	156.2	108.7	107.7	109.5
C4−C5−O5−C1	45.6	45.9	46.8	−18.2	−15.1	−17.6	59.9	60.5	59.9
C5−O5−C1−H1	−171.5	−170.6	−171.9	164.6	166.8	163.8	54.5	54.6	55.4
C5−O5−C1−O1	68.5	69.2	67.7	105.6	104.9	105.4	25.6	27.5	27.5
C5−O5−C1−O_{Ser}	−150.3	−151.2	−151.3	−97.0	−99.2	−97.5	173.0	173.5	174.1
H2−C2−N−H_{NAc}	149.1	148.4	149.0	175.3	177.2	174.9	178.4	179.7	179.0
Q(C1)	0.415	0.408	0.370	0.497	0.489	0.449	0.819	0.821	0.851
Q(O1)	−0.543	−0.535	−0.534	−0.808	−0.815	−0.805	−0.856	−0.851	−0.802
Q(O_{Ser})	−0.868	−0.862	−0.874	−0.908	−0.913	−0.874	−0.900	−0.928	−0.937
Q(O5)	−0.489	−0.514	−0.481	−0.354	−0.324	−0.352	−0.668	−0.673	−0.677
Q(C2)	0.141	0.093	0.150	0.679	0.645	0.696	0.283	0.255	0.204
Q(C5)	0.164	0.176	0.134	0.041	0.018	0.025	−0.039	−0.030	0.041
Q(N_{His})	−0.149	−0.120	−0.118	−0.317	−0.299	−0.287	−0.203	−0.159	−0.207
Q(H1)	0.106	0.124	0.115	−0.160	−0.156	−0.145	−0.028	−0.035	−0.069
Q(HO_{Ser})	0.236	0.240	0.246	0.399	0.382	0.380	0.354	0.351	0.394
Q(HN_{Ac})	0.415	0.180	0.171	0.279	0.238	0.258	0.123	0.092	−0.015

map. One along the axes represents a stepwise mechanism, with the first step representing dissociation of the C1−O1 glycosidic linkage (r_2) and leading to the oxocarbenium ion (C). The second step, along the *x*-axis, represents the nucleophilic attack by the protonated O_{Ser} on the C1 and the creation of a new glycosidic linkage (INT). A review of the structures along this path revealed that the proton H_{Ser} remains on the O_{Ser}, which means that the final structure is not the product but the structure with protonated glycosidic oxygen. To complete the reaction, this proton needs to be transferred to the catalytic base His498. The transition barrier (B12a) to the oxocarbenium ion (C) of ∼48 kcal mol^{-1} is located at $r_{C1-O1} \approx 2.5$ Å, and the relative energy of the oxocarbenium ion is ∼24 kcal mol^{-1}. The next step has a transition barrier (B12b) of ∼9 kcal mol^{-1}, and the relative energy of the protonated product is ∼28 kcal mol^{-1}. The alternative pathway follows the diagonal of the two-dimensional map connecting the ES and the product with the protonated oxygen O_{Ser}. A transition barrier (B12) of ∼34 kcal mol^{-1} was detected in the central area of the contour map and is located at $r_1 \approx 1.7$ Å and $r_2 \approx 3.0$ Å. Each of these two pathways has a barrier which is significantly larger than the one observed at the (r_1,r_3) PES. The location of the B12 barrier also coincides with the C1−O_{Ser} and C1−O1 distances determined in the transition barrier structure B13 observed in Figure 2. This is quite interesting and further supports a strong correlation between the r_1 (C1−O_{Ser}) and r_2 (C1−O1) distances.

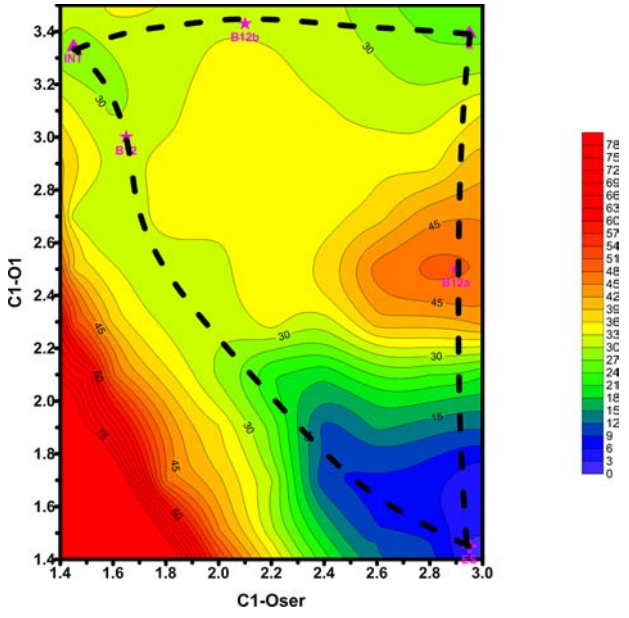

Figure 4. PES calculated at the B3LYP/6-31G* level using distances r_1 and r_2 as reaction coordinates. The black dashed lines indicate two alternative reaction pathways; the one parallel to the axes represents a stepwise mechanism, and the second, along the diagonal, represents a concerted mechanism.

dx.doi.org/10.1021/ja307040m | J. Am. Chem. Soc. 2012, 134, 15563−15571

PES as a Function of the r_2 (r_{C1-O1}) and r_3 ($r_{H_{Ser}-N_{His}}$) Distances. Figure 5 shows the PES calculated as a function of the distance between C1 and the O1 oxygen atom of the donor GlcNAc residue (r_2) and the distance between the H_{Ser} proton and the N_{His} nitrogen atom of the catalytic base (r_3). The energy contours in Figure 5 show that a change of one reaction coordinate does not influence behavior of the second one, and the proton transfer and dissociation of the C1−O1 bond are quite independent. The structure in the upper right corner represents the oxocarbenium ion. However, we did not localize the oxocarbenium ion as a local minimum, and the structures appear to have high energy. An examination of the geometrical changes showed that the r_1 reaction coordinate did not change during dissociation of the C1−O1 bond.

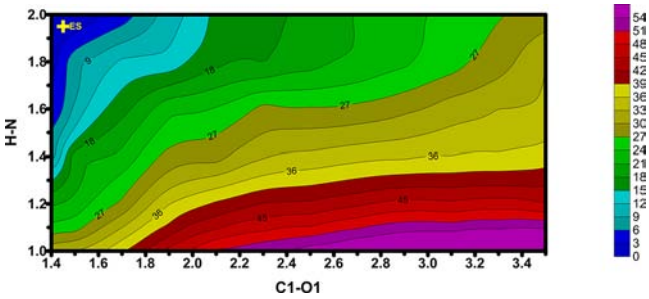

Figure 5. PES calculated at the B3LYP/6-31G* level using distances r_2 and r_3 as reaction coordinates.

Our calculations of the (r_1,r_2), (r_1,r_3), and (r_2,r_3) energy surfaces clearly show how the equilibrium r_{C1-O1} distance elongates with the shortening of $r_{C1-O_{Ser}}$. On the other hand, we did not observe the reverse effect of r_2 on r_1.

On the Catalytic Mechanism of OGT. Structure and kinetics experiments[14] on OGT support the ordered bi-bi catalytic mechanism, with His498 proposed as the catalytic base for OGT. In this mechanism, the UDP-GlcNAc binds first, and interactions between the α-phosphate of the UDP moiety and the backbone amide of the glycosylated serine help to align the CKII peptide, which then binds over the nucleotide sugar. An ordered bi-bi mechanism with UDP-GlcNAc binding first and

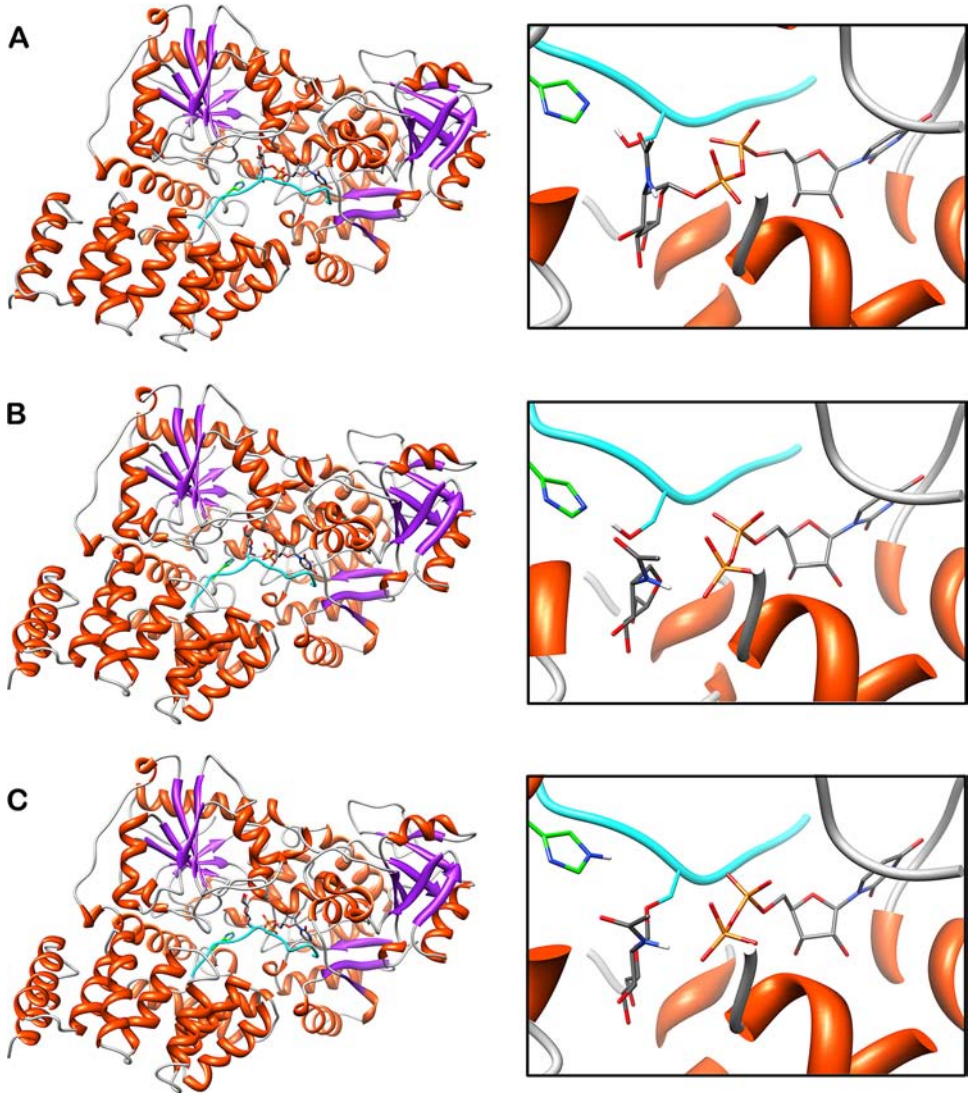

Figure 6. Active-site models for (A) the Michaelis complex (ES), (B) the transition state (TS), and (C) the product complex (P) calculated at the B3LYP level. Left, overall view of OGT complex; right, close-up of the active site, with the acceptor shown in cyan.

dx.doi.org/10.1021/ja307040m | J. Am. Chem. Soc. 2012, 134, 15563−15571

UDP leaving last is supported by the observation that UDP is found to be a competitive inhibitor of UDP-GlcNAc.[14]

In general, previous calculations on inverting glycosyltransferases of the GT-A family support a S_N2-like mechanism, in which the enzyme provides a catalytic base that activates the nucleophile to displace the UDP leaving group from the nucleotide sugar (donor) in a concerted process.[15,17] This study is the first calculation for an inverting ion-independent glycosyltransferase from the GT-B family, and the calculated two-dimensional sections of PES characterized by the predefined reaction coordinates (r_1, r_2, r_3) clearly showed that the energetically preferred mechanism started with the nucleophilic attack. This suggests that OGT employs a S_N2-like mechanism, in which a nucleophilic attack by O_{Ser} (r_1), facilitated by the proton transfer to the catalytic base (r_3), and the dissociation of the leaving group (r_2) occur almost simultaneously.

A comparison of the calculated reaction barriers with experimental data supports this. To our knowledge, only two k_{cat} values, 0.22 and 0.29 min^{-1}, have been reported[14] for OGT. These values are in the range of k_{cat} values observed for blood group A and B glycosyltransferases[49] and for FucT V,[50] from 50 to 0.1 s^{-1}. Using the phenomenological description associating k_{cat} with the activation free energy, $\Delta G^{cat} = -RT\ln(hk_{cat}/k_BT)$, an activation barrier of 21 kcal mol^{-1} has been determined for OGT. This estimate is in reasonable agreement with the overall activation energies of 15.6, 19.6, and 15.5 kcal mol^{-1} calculated at the B3LYP, MPW1K, and M06-2X levels, respectively, for the GlcNAc transfer mechanism via the [ES→TS→P] pathway (Figure 6 and Table 2).

The single-point energy barriers are between 13 and 22 kcal mol^{-1}. (Energies in hartrees for the stationary points are available in Supporting Information.) The barriers calculated at the B3LYP and M06-2X levels are somewhat lower that those obtained with other functionals. Comparison of TS structures calculated at the B3LYP, MPW1K, and M06-2X levels shows that the TS search led essentially to the same TS structure (Table 1). The TS structure at the B3LYP (MPW1K, M06-2X) level is characterized by the distances r_1 = 1.842 (1.924, 1.819) Å, r_2 = 3.214 (3.109, 3.173) Å, and r_3 = 1.610 (1.679, 1.613) Å. The geometry of the ES model at the B3LYP (MPW1K, M06-2X) level is characterized by values of 1.461 (1.436, 1.444) and 1.379 (1.367, 1.377) Å for the C1−O1 and C1−O5 bond lengths, respectively. Thus, in the TS, the C1−O1 scissile linkage significantly differs from that in the ES and increases drastically by almost 2 Å, going from 1.461 (1.436, 1.444) to 3.214 (3.109, 3.173) Å. In contrast, the C1−O5 bond shortens from 1.379 (1.367, 1.377) to 1.307 (1.278, 1.303) Å. The pyranoid ring of the GlcNAc in the ES and P is in the $^4C_1$ chair conformation characterized by ring-puckering parameters ϕ = 140.1°, θ = 11.3°, and Q = 0.50 (139.8°, 11.2°, 0.49; 139.5°, 10.8°, 0.50) and ϕ = 100.4°, θ = 3.7°, and Q = 0.59 (107.6°, 2.9°, 0.59; 116.0°, 2.8°, 0.59), respectively. The conformation of the pyranoid ring is a $^4H_3$ half-chair in TS, with puckering parameters at the B3LYP (MPW1K, M06-2X) level ϕ = 192.3°, θ = 69.4°, and Q = 0.57 (191.7°, 66.7°. 0.55; 192.6°, 68.9°, 0.57). The TS structure calculated at the MPW1K level is shown in Figure 7. The changes in the ring conformation are accompanied by changes in a charge distribution at the reaction center C1. In the TS, the atoms attached to the anomeric carbon C1 become coplanar with sp^2 character. The oxocarbenium ion-like character is stabilized by delocalization of the ring oxygen lone-pair electrons into the empty p orbital at C1. This is reflected in shortening C1−O5 bond length and changes in a charge distribution (Table 1). Comparison of ESP shows that, on going from ES to TS, the negative charge on O5 decreases as a consequence of this delocalization. Although ΔG values would be more appropriate for a description of the reaction processes, our conclusions are based on the energy values. For a complex with 198 atoms in the QM region and almost 11 400 in the MM region, a proper determination of ΔG for each step of the catalytic reaction would require a massive computational resource. However, our past experience working with GT models suggests that the inclusion of the zero-point energy and thermodynamic contributions to the calculated energies would only slightly alter the energy differences. Therefore, we did not perform such calculations. The investigation of all of these aspects was beyond the scope of this work.

Table 2. QM/MM Energies (kcal mol^{-1}) of the Michaelis Complex (ES) and the Relative Energies of the Transition State (TS) and Product Complex (P) for the S_N2 Reaction Pathway Calculated at Various Levels of Theory Using the 6-31G Basis Set with Diffuse Functions (6-31+G**) on O1′, O5′, O_{Ser21}, and N_{His498} Atoms and with the MM Subsystem Characterized with an OPLS_2005 All-Atom Force Field**

method	geometry	ES	TS	P
B3LYP	B3LYP	−3 505 657.48	15.60	−1.74
PWB6K		−3 507 360.32	21.40	0.30
MPW1K		−3 504 808.35	22.40	−1.89
M06-2X		−3 504 425.97	16.12	−0.78
M05-2X		−3 505 327.98	15.60	−0.74
MPW1K	MPW1K	−3 504 821.94	19.57	−6.20
B3LYP		−3 505 644.64	15.15	−0.13
PWB6K		−3 507 378.25	16.38	−5.12
M06-2X		−3 504 420.97	12.84	−4.30
M05-2X		−3 505 326.43	14.39	−3.78
M06-2X	M06-2X	−3 504 430.42	15.47	−7.28
B3LYP		−3 505 653.80	13.81	4.99
PWB6K		−3 507 370.19	20.24	−3.09
MPW1K		−3 504 815.28	20.53	−0.49
M05-2X		−3 505 331.26	14.44	−3.71

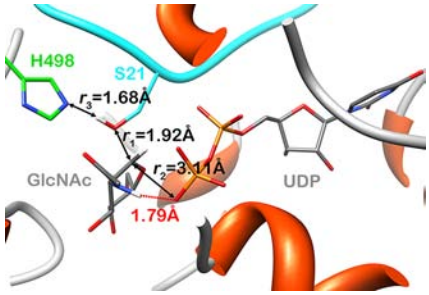

Figure 7. QM(MPW1K)/MM(OPLS_2005) optimized TS structure. The donor, acceptor, and catalytic base are shown in stick representation. Relevant distances (in Å) are indicated in black. The interaction between the H_{NAc} and O1 atoms is indicated by the red dotted line, and distance (in Å) is shown in red.

The calculations also revealed that OGT employs an acetamido group at the position adjacent to the anomeric bond to facilitate the cleavage of the glycosidic linkage by stabilizing the developing negative charge. It is interesting to note that OGA, a glycoside hydrolase involved in *O*-GlcNAcylation cycling, uses an acetamido group as a nucleophile to cleave GlcNAc from serine/threonine.[51] The same mechanism is used by a number of glycoside hydrolase families, but the involvement of a neighboring group from a donor in the catalytic mechanism was observed for the first time with glycosyltransferases.

The QM/MM calculations on the catalytic mechanism of two glycosyltransferases from the GT-A superfamily, GnT-I[16] and β4Gal-T1,[19] revealed that a primary hydroxyl group (Ob6-H) from the acceptor interacts with the oxygen from the phosphate group and plays a role in stabilizing TS and also in facilitating the departure of the leaving group. This finding for GnT-I is supported by experimental data. They showed that removal of the Cb6 hydroxyl group decreases the activity of GnT-I and that the Ob6-methylated acceptor is a substrate but has no catalytic activity.[52] With OGT, the acceptor is a serine/threonine amino acid residue and, due to a lack of hydroxyl groups, such interactions are not possible. Additionally, OGT is a metal-ion-independent enzyme and therefore cannot employ a divalent cation in its catalytic mechanism. Our finding suggests that, to overcome these structural factors, OGT has developed a novel mechanism that involves an acetamido group at the position adjacent to the reactive anomeric center, similarly to OGA. In OGT, the role of the NAc group is to facilitate the formation of the glycosidic bond. In contrast, in OGA the NAc group facilitates the breaking of the glycosidic linkage. Though it may be coincidental that both enzymes use the NAc group of the donor GlcNAc in the so-called substrate-assisted mechanism, the fact that OGT and OGA are both involved in *O*-GlcNAcylation cycling supports this conclusion and indicates that OGA and OGT might have evolved to preferentially use this NAc group in their catalytic mechanism. This kind of participation in the catalytic mechanism of glycoside hydrolases was termed the neighboring-group or substrate-assisted mechanism,[51] and we proposed to use the same name for OGT. Of course, verification of this hypothesis awaits further experimental and theoretical studies, and it would be premature to entirely exclude the possibility of the catalytic reaction proceeding via another pathway.

CONCLUSION

Despite its extreme importance, the mechanism of OGT has not yet been determined. This study uses QM/MM methods to explore the potential energy surface for the transfer of GlcNAc to serine by the inverting *N*-acetylglucosaminyltransferase OGT. The structural model of the reaction site used in this paper is based on the crystal structures of OGT.[14] The entire enzyme−substrate system (OGT-UDP-GlcNAc-CKII peptide ternary complex, altogether 11 524 atoms) was partitioned into two different subsystems: the QM subsystem, containing 198 atoms, and the MM region, containing 11 326 atoms. This is the first calculation on an inverting ion-independent glycosyltransferase from the GT-B family. These results shed some light on the catalytic mechanism of OGT. The calculations revealed that nucleophilic attack, dissociation of the C1−O1 glycosidic linkage, and proton transfer from nucleophile oxygen to catalytic base all occur simultaneously and support the S_N2-like substrate-assisted mechanism in which the NAc group of GlcNAc assists in breaking the glycosidic linkage and the departure of the leaving group (UDP).

ASSOCIATED CONTENT

Supporting Information

QM/MM atomic coordinates (.pdb) and energies in hartrees for all stationary points calculated at the B3LYP, MPW1K, and M06-2X levels. This material is available free of charge via Internet at http://pubs.acs.org.

AUTHOR INFORMATION

Corresponding Author

chemitsa@savba.sk

Notes

The authors declare no competing financial interest.

[⊥]S.K. is on leave from the Institute of Chemistry, Slovak Academy of Sciences, Bratislava, Slovakia.

ACKNOWLEDGMENTS

The research leading to these results obtained financial contribution from the European Union under the Seventh Framework Programme by CEITEC (CZ.1.05/1.1.00/02.0068) project from European Regional Development Fund, SYLICA (Contract No. 286154 under "Capacities" specific programme) and SoMoPro (No. 2SGA2747, under the FP/2007-2013 grant agreement No. 229603) programme, and the Ministry of Education of the Czech Republic (ME 08008). The research is also co-funded by the South Moravian region. The authors thank the Czech National Supercomputing Centre, METACENTRUM, for providing computational resources. Access to the MetaCentrum computing facilities is provided under the research intent MSM6383917201. This work was also supported by the Scientific Grant Agency of the Ministry of Education of Slovak Republic and Slovak Academy of Sciences (grants VEGA-02/0159/12 and VEGA-02/0161/12) and Research & Development Operational Programmes funded by the ERDF (Centre of Excellence on Green Chemistry Methods and Processes, CEGreenI, Contract No. 26240120001, and Amplification of the Centre of Excellence on Green Chemistry Methods and Processes, CEGreenII, Contract No. 26240120025). We thank Shinya Fushinobu for an access to the Cremer−Pople parameter calculator (hi-ho).

REFERENCES

(1) Torres, C. R.; Hart, G. W. *J. Biol. Chem.* **1984**, *259*, 3308−3317.
(2) Copeland, R. J.; Bullen, J. W.; Hart, G. W. *Am. J. Physiol. Endocrinol. Metab.* **2008**, *295*, E17−E28.
(3) Hanover, J. A. *FASEB J.* **2001**, *15*, 1865−1876.
(4) Hart, G. W.; Housley, M. P.; Slawson, C. *Nature* **2007**, *446*, 1017−1022.
(5) Hart, G. W.; Slawson, C.; Ramirez-Correa, G.; Lagerlof, O. In *Annuual Reviews in Biochemistry*; Kornberg, R. D., Raetz, C. R. H., Rothman, J. E., Thorner, J. W., Eds.; Annual Reviews: Palo Alto, CA, 2011; Vol. *80*, pp 825−858.
(6) Wells, L.; Vosseller, K.; Hart, G. W. *Science* **2001**, *291*, 2376−2378.
(7) Hurtado-Guerrero, R.; Dorfmueller, H. C.; Van Aalten, D. M. *Curr. Opin. Struct. Biol.* **2008**, *18*, 551−557.
(8) Martinez-Fleites, C.; He, Y.; Davies, G. J. *Biochim. Biophys. Acta Gen. Subj.* **2010**, *1800*, 122−133.
(9) Haltiwanger, R. S.; Blomberg, M. A.; Hart, G. W. *J. Biol. Chem.* **1992**, *267*, 9005−9013.
(10) Butkinaree, C.; Park, K.; Hart, G. W. *Biochim. Biophys. Acta Gen. Subj.* **2010**, *1800*, 96−106.

(11) Zeidan, Q.; Hart, G. W. *J. Cell Sci.* **2010**, *123*, 13−22.
(12) Cantarel, B. L.; Coutinho, P. M.; Rancurel, C.; Bernard, T.; Lombard, V.; Henrissat, B. *Nucleic Acids Res.* **2009**, *37*, D233−D238.
(13) Wrabl, J. O.; Grishin, N. V. *J. Mol. Biol.* **2001**, *314*, 365−374.
(14) Lazarus, M. B.; Nam, Y. S.; Jiang, J. Y.; Sliz, P.; Walker, S. *Nature* **2011**, *469*, 564−U168.
(15) Lairson, L. L.; Henrissat, B.; Davies, G. J.; Withers, S. G. *Annu. Rev. Biochem.* **2008**, *77*, 521−555.
(16) Kozmon, S.; Tvaroska, I. *J. Am. Chem. Soc.* **2006**, *128*, 16921−16927.
(17) Tvaroska, I. *Mini-Rev. Org. Chem.* **2011**, *8*, 263−269.
(18) Tvaroska, I.; Andre, I.; Carver, J. P. *Glycobiology* **2003**, *13*, 1−8.
(19) Krupicka, M.; Tvaroska, I. *J. Phys. Chem. B* **2009**, *113*, 11314−11319.
(20) Sali, A. *MODELLER*, A Program for Protein Structure Modeling, v.9.9; University of California: San Francisco, 2011.
(21) Sali, A.; Blundell, T. L. *J. Mol. Biol.* **1993**, *234*, 779−815.
(22) Pettersen, E. F.; Goddard, T. D.; Huang, C. C.; Couch, G. S.; Greenblatt, D. M.; Meng, E. C.; Ferrin, T. E. *J. Comput. Chem.* **2004**, *25*, 1605−1612.
(23) *Maestro*, v.9.2; Schrodinger, LLC: New York, 2011.
(24) *Epik*, v.2.2; Schrodinger, LLC: New York, 2011.
(25) *Impact*, v.5.7; Schrodinger, LLC: New York, 2011.
(26) *Prime*, v.3.0; Schrodinger, LLC: New York, NY, 2011.
(27) *Schrodinger Suite 2011*, Protein Preparation Wizard; Schrodinger, LLC: New York, 2011.
(28) Glide, 5.7; Schrodinger, LLC: New York, 2011.
(29) Friesner, R. A.; Banks, J. L.; Murphy, R. B.; Halgren, T. A.; Klicic, J. J.; Mainz, D. T.; Repasky, M. P.; Knoll, E. H.; Shelley, M.; Perry, J. K.; Shaw, D. E.; Francis, P.; Shenkin, P. S. *J. Med. Chem.* **2004**, *47*, 1739−1749.
(30) Friesner, R. A.; Murphy, R. B.; Repasky, M. P.; Frye, L. L.; Greenwood, J. R.; Halgren, T. A.; Sanschagrin, P. C.; Mainz, D. T. *J. Med. Chem.* **2006**, *49*, 6177−6196.
(31) Halgren, T. A.; Murphy, R. B.; Friesner, R. A.; Beard, H. S.; Frye, L. L.; Pollard, W. T.; Banks, J. L. *J. Med. Chem.* **2004**, *47*, 1750−1759.
(32) Park, M. S.; Gao, C.; Stern, H. A. *Proteins: Struct., Funct. Bioinform.* **2011**, *79*, 304−314.
(33) Jorgensen, W. L.; Maxwell, D. S.; TiradoRives, J. *J. Am. Chem. Soc.* **1996**, *118*, 11225−11236.
(34) *Jaguar*, v.7.8; Schrodinger, LLC: New York, 2011.
(35) Becke, A. D. *J. Chem. Phys.* **1993**, *98*, 5648−5652.
(36) Lee, C. T.; Yang, W. T.; Parr, R. G. *Phys. Rev. B* **1988**, *37*, 785−789.
(37) *QSite*, v.5.7; Schrodinger, LLC: New York, 2011.
(38) Murphy, R. B.; Philipp, D. M.; Friesner, R. A. *J. Comput. Chem.* **2000**, *21*, 1442−1457.
(39) Philipp, D. M.; Friesner, R. A. *J. Comput. Chem.* **1999**, *20*, 1468−1494.
(40) Zhao, Y.; Truhlar, D. G. *Theor. Chem. Acc.* **2008**, *120*, 215−241.
(41) Lynch, B. J.; Fast, P. L.; Harris, M.; Truhlar, D. G. *J. Phys. Chem. A* **2000**, *104*, 4811−4815.
(42) Zhao, Y.; Truhlar, D. G. *J. Phys. Chem. A* **2005**, *109*, 5656−5667.
(43) Zhao, Y.; Schultz, N. E.; Truhlar, D. G. *J. Chem. Theory Comput.* **2006**, *2*, 364−382.
(44) Xu, X. F.; Alecu, I. M.; Truhlar, D. G. *J. Chem. Theory Comput.* **2011**, *7*, 1667−1676.
(45) Zheng, J. J.; Zhao, Y.; Truhlar, D. G. *J. Chem. Theory. Comput.* **2009**, *5*, 808−821.
(46) Tvaroska, I.; Andre, I.; Carver, J. P. *J. Am. Chem. Soc.* **2000**, *122*, 8762−8776.
(47) Tvaroska, I. *Trends Glycosci. Glycobiol.* **2005**, *17*, 177−190.
(48) Fowler, P.; Bernet, B.; Vasella, A. *Helv. Chim. Acta* **1996**, *79*, 269−287.
(49) Seto, N. O. L.; Compston, C. A.; Evans, S. V.; Bundle, D. R.; Narang, S. A.; Palcic, M. M. *Eur. J. Biochem.* **1999**, *259*, 770−775.
(50) Murray, B. W.; Takayama, S.; Schultz, J.; Wong, C.-H. *Biochemistry* **1996**, *35*, 11183−11195.
(51) Vocadlo, D. J.; Withers, S. G. *Biochemistry* **2005**, *44*, 12809−12818.
(52) Schachter, H.; Reck, F.; Paulsen, H. *Methods Enzymol.* **2003**, *363*, 459−475.